FORMATION AND EVOLUTION OF COROTATING INTERACTION REGIONS AND THEIR THREE DIMENSIONAL STRUCTURE

J. T. GOSLING[1] AND V. J. PIZZO[2]
[1]*Los Alamos National Laboratory, Los Alamos, New Mexico, USA*
[2]*Space Environment Center, NOAA, Boulder, Colorado, USA*

Received: 31 August 1998; Accepted: 8 April 1999

Abstract. Corotating interaction regions are a consequence of spatial variability in the coronal expansion and solar rotation, which cause solar wind flows of different speeds to become radially aligned. Compressive interaction regions are produced where high-speed wind runs into slower plasma ahead. When the flow pattern emanating from the Sun is roughly time-stationary these compression regions form spirals in the solar equatorial plane that corotate with the Sun, hence the name corotating interaction regions, or CIRs. The leading edge of a CIR is a forward pressure wave that propagates into the slower plasma ahead, while the trailing edge is a reverse pressure wave that propagates back into the trailing high-speed flow. At large heliocentric distances the pressure waves bounding a CIR commonly steepen into forward and reverse shocks. Spatial variation in the solar wind outflow from the Sun is a consequence of the solar magnetic field, which modulates the coronal expansion. Because the magnetic equator of the Sun is commonly both warped and tilted with respect to the heliographic equator, CIRs commonly have substantial north-south tilts that are opposed in the northern and southern hemispheres. Thus, with increasing heliocentric distance the forward waves in both hemispheres propagate toward and eventually across the solar equatorial plane, while the reverse shocks propagate poleward to higher latitudes. This paper provides an overview of observations and numerical models that describe the physical origin and radial evolution of these complex three-dimensional (3-D) heliospheric structures.

1. Introduction

1.1. Magnetic Control of the Solar Wind Expansion

The solar wind is a consequence of the supersonic expansion of the Sun's hot outer atmosphere, the solar corona (*e.g.*, Parker, 1963). The solar magnetic field that permeates the corona strongly modulates this expansion (*e.g.*, Pneuman and Kopp, 1971). Indeed, it is the interplay between the coronal magnetic field and the expansion that produces both a highly structured solar corona and a spatially variable solar wind. To a first approximation the magnetic field in the corona well above the photosphere is roughly that of a dipole tilted with respect to the rotation axis of the Sun. The tilt varies as the solar magnetic field evolves through the 11-year solar activity cycle. As illustrated in the left panel of Fig. 1, the dipole tends to be inclined substantially relative to the solar rotation axis on the declining phase of the solar cycle, whereas it tends to be nearly aligned with the rotation axis near

Space Science Reviews **89:** 21–52, 1999.

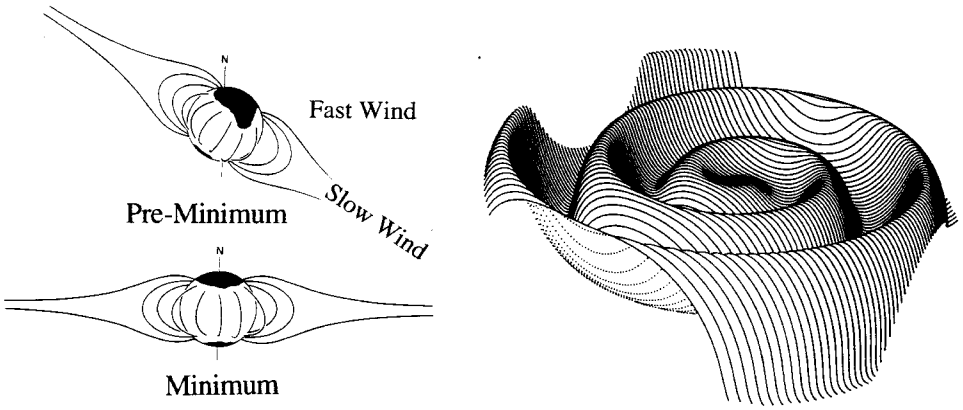

Figure 1. Left panel: Schematic illustrating the changing tilt of the solar magnetic dipole and coronal structure relative to the rotation axis of the Sun, as well as the origin of high and low-speed solar wind flows. *Right panel:* Idealized configuration of the heliospheric current sheet in interplanetary space when the tilt of the solar magnetic dipole is substantial (adapted from Hundhausen, 1977, and Jokipii and Thomas, 1981).

solar activity minimum (*e.g.*, Hundhausen, 1977). Near solar activity maximum the solar magnetic field is sufficiently complex that the dipole concept is probably not useful.

Near the magnetic equator and immediately above the solar photosphere the magnetic field is transverse to the radial direction and is sufficiently strong to constrain the plasma from expanding outward. Thus closed magnetic field arcades commonly straddle the magnetic equator, as illustrated in the left panel of Fig. 1. At greater heights in the solar atmosphere the field weakens sufficiently that the arcades are opened up by the pressure of the coronal plasma, and the plasma is free to expand outward. The resulting outflow produces helmet-like streamers in the corona and a relatively slow and dense solar wind flow far from the Sun (*e.g.*, Gosling *et al.*, 1981; Feldman *et al.*, 1981). Embedded within the low-speed flow is a magnetic field polarity reversal, reflecting the magnetic control of the expansion. At higher magnetic latitudes the coronal expansion is relatively unconstrained by the magnetic field. The resulting expansion produces regions of low density in the solar atmosphere known as coronal holes (*e.g.*, Krieger *et al.*, 1973) and high-speed flows in the heliosphere that are both unipolar and of relatively low density.

1.2. The Heliospheric Current Sheet

The polarity reversal, which is found within the low-speed wind and which maps back to the solar magnetic equator, is commonly called the heliospheric current sheet (HCS). Near solar minimum the HCS tends to coincide roughly with the

solar equatorial plane, although some warping is almost always present. On the other hand, during the approach to solar minimum when the magnetic dipole is strongly tilted relative to the solar rotation axis, solar rotation and the solar wind flow bend the HCS into a configuration similar to that shown in the right panel of Fig. 1. The maximum solar latitude attained by the HCS in this simple picture is the same as the tilt of the magnetic dipole relative to the solar rotation axis. As will be seen, corotating interaction regions are tilted in the same sense as is the HCS because both arise from basically the same geometry back at the Sun. It is worth remembering, of course, that the solar magnetic field is never actually a simple dipole; moreover, as we shall see, dynamic processes in the solar wind eventually severely distort the shape of the HCS. Thus the HCS is usually considerably more complex than illustrated in Fig. 1.

1.3. Latitudinal Variation of the Solar Wind Flow

Observations reveal that solar wind properties vary strongly with distance from the HCS, with flow speed increasing and density decreasing away from the current sheet (*e.g.*, Zhao and Hundhausen, 1981; Bruno *et al.*, 1986). Thus, because the solar magnetic equator is commonly warped as well as tilted with respect to the heliographic equator, both low and high-speed flows are commonly observed at low heliographic latitudes as the Sun rotates. On the declining phase of the solar cycle and near solar activity minimum solar wind variability is confined almost entirely to a relatively narrow latitude band centered on the heliographic equator (Schwenn, 1990; Gosling *et al.*, 1995b), while at high latitudes a nearly constant wind with speed of about 750 km/s and density (scaled to Earth's orbit) of about 2.5 cm^{-3} prevails (Phillips *et al.*, 1994). This is illustrated in Fig. 2, which shows solar wind speed as a function of solar latitude as measured by Ulysses during its first polar orbit about the Sun extending from February 1992 through December 1997 on the declining phase and at the minimum of the most recent solar cycle (#22). The width of the band of solar wind variability changes as both the warping of the magnetic equator and the tilt of the dipole change. Ulysses observations indicate that the width of the band of solar wind variability ranged from about $\pm 20^\circ$ to $\pm 35^\circ$ in latitude in the years leading up to and including the most recent solar minimum (Gosling *et al.*, 1995b; Gosling *et al.*, 1997), consistent with earlier estimates based upon observations of the interplanetary scintillation of astronomical radio sources (*e.g.*, Coles, 1995). We expect that the band of wind variability extends to significantly higher heliographic latitudes near the maximum of the solar activity cycle.

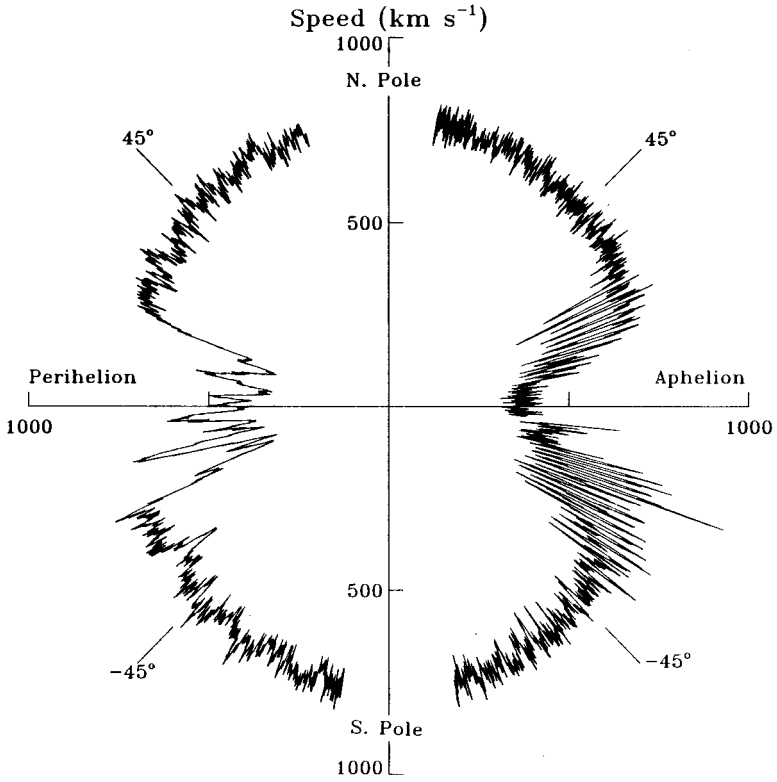

Figure 2. Solar wind speed as a function of heliographic latitude measured by Ulysses. Data shown in the left portion of the figure are centered on orbit perihelion at 1.4 AU, while data on the right are centered on orbit aphelion at 5.4 AU. The apparent difference in the latitude scale of structure in the flow speed at perihelion and aphelion is an artifact associated with the fact that the spacecraft changed latitude very rapidly near perihelion but very slowly near aphelion.

2. Formation of Corotating Interaction Regions

As the Sun rotates, flows of different speed become radially aligned within the low-latitude band of solar wind variability. Faster wind runs into slower wind ahead while simultaneously outrunning slower trailing wind. Since these radially aligned parcels of plasma originate from different positions on the Sun at different times, they are threaded by different magnetic field lines and are thus prevented from interpenetrating. As a result, a compression forms on the rising-speed portion of a high-speed stream and a rarefaction forms on the trailing edge (*e.g.*, Parker, 1963; Sarabhai, 1963; Carovillano and Siscoe, 1969; Hundhausen, 1972). The compressions and related phenomena provide the focus of the present volume. Because the pattern of compression rotates with the Sun when the outflow from the Sun is time stationary, these high pressure regions are known as corotating interaction regions, or CIRs (Smith and Wolfe, 1976).

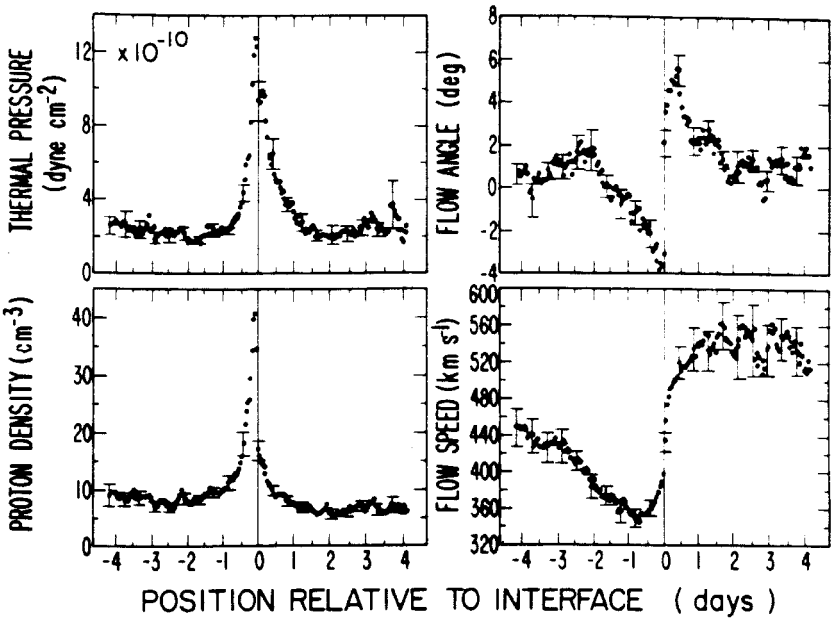

Figure 3. Superposed epoch plots of selected 1-hour averaged solar wind parameters for 23 CIRs containing abrupt stream interfaces. The flow angle is the azimuthal (east-west) flow angle and the sign convention is that negative flow angles correspond to flow in the direction of planetary motion about the Sun (westward) (from Gosling *et al.*, 1978).

3. Corotating Interaction Regions at Earth's Orbit

The interaction between fast and slow solar wind begins in the inner heliosphere (*e.g.*, Richter and Luttrell, 1986); CIRs thus are commonly well formed at Earth's orbit, one astronomical unit (AU) from the Sun (*e.g.*, Siscoe, 1972; Gosling *et al.*, 1972). The characteristic appearance of CIRs at 1 AU is illustrated in Fig. 3, which shows the result of a superposed epoch analysis of data obtained at 1 AU during 23 CIRs. All 23 of the CIRs chosen for the analysis contained well-defined stream interfaces, which were used to define the zero epoch in the analysis. (Stream interfaces are distinguished as abrupt and simultaneous drops in particle density and rises in proton temperature within CIRs (*e.g.*, Belcher and Davis, 1971; Burlaga, 1974; Gosling *et al.*, 1978). They separate what was originally slow, dense plasma from what was originally fast thin plasma back at the Sun (Gosling *et al.*, 1978; Wimmer-Schweingruber *et al.*, 1997). It is apparent that the pressure within a CIR peaks in the vicinity of the interface, which is also the site of a large shear in the flow. The slow dense plasma ahead of the interface is deflected in the sense of planetary motion about the Sun (negative flow azimuth), while the less dense plasma behind the interface is deflected in the opposite direction.

4. A Simple Model of the Radial Evolution of a Corotating Interaction Region

Figure 4, which shows the result of a calculation using a one-dimensional (1-D, spherically symmetric), adiabatic, gas dynamic code, shows how high-speed streams and their related CIRs evolve with increasing distance from the Sun (Hundhausen, 1973). The calculation extends from an inner boundary at 0.14 AU, which lies outside the critical point where the solar wind turns supersonic, to an outer boundary at 3.0 AU. Speed, density, and temperature were first held steady at the inner boundary until a stationary, supersonic flow with a flow speed of 325 km/s at 3.0 AU filled the computational mesh; then a high-speed stream was introduced into the calculation by linearly increasing and then decreasing the temperature (and thus also the pressure) by a factor of four at the inner boundary over a period of 100 hours. This produced an enhanced outflow from the Sun of finite duration. The figure shows temporal snapshots of flow speed (above) and pressure (below) as functions of heliocentric distance. Thus it shows these quantities at various heliocentric distances both initially and at later times when the evolution of the high-speed stream and the CIR is dominated by the nonlinear steepening of the speed profile. The leading portion of the stream steepens with increasing heliocentric distance because the peak of the stream is traveling faster than the slower plasma ahead. As the speed profile steepens, material within the stream is rearranged; parcels of plasma on the rising-speed portion of the stream are compressed to form the high pressure interaction region, while parcels of plasma on the falling-speed portion of the stream are increasingly separated, producing a rarefaction. The temporal variations of solar wind speed, density, and pressure observed within high-speed streams and CIRs at 1 AU (*e.g.*, Gosling *et al.*, 1972; Gosling *et al.*, 1978) are in reasonable agreement with simple calculations such as these (see Fig. 3); the agreement improves when the magnetic field and the additional dimensions are added to the calculation.

Being a region of high pressure, the interaction region expands into the plasma both ahead and behind at the fast mode speed (actually at the sound speed in the calculation shown in Fig. 4). The leading edge of the CIR is called a forward wave, while the trailing edge is called a reverse wave. Pressure gradients associated with these waves produce an acceleration of the slow wind ahead of the stream and a deceleration of the fast wind within the stream. The net effect of the interaction is to limit the steepening of the stream and to transfer momentum and energy from the fast wind to the slow wind. When the difference in speed between the fast and the slow wind is greater than about twice the fast mode (sound) speed, the stream initially steepens faster than the interaction region can expand into the surrounding plasma so that at first the interaction region squeezes down with increasing heliocentric distance (Hundhausen, 1973). The nonlinear rise in pressure associated with this squeezing eventually causes the forward and reverse waves bounding the interaction region to steepen into shocks. Since shocks propagate

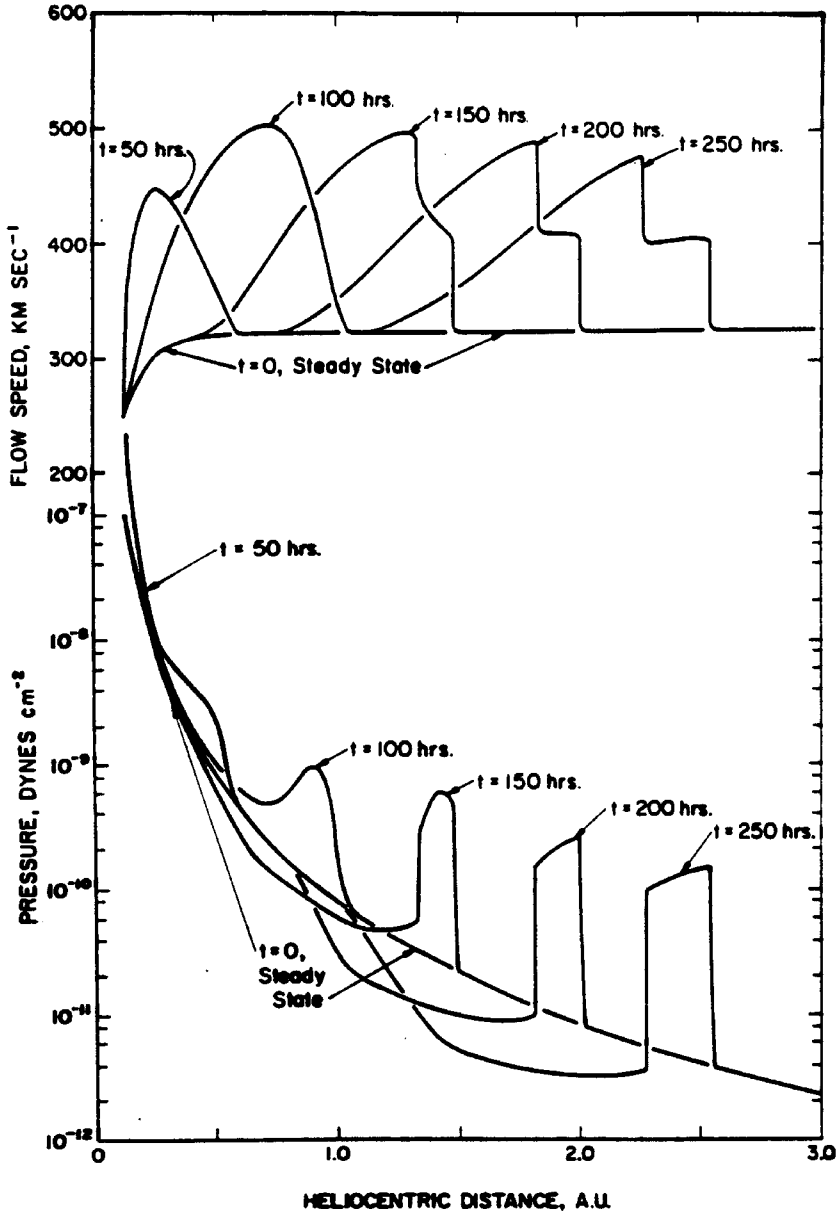

Figure 4. Snapshots of solar wind flow speed and pressure as functions of heliocentric distance at different times during the outward evolution of a high-speed stream as calculated from a simple 1-D gas dynamic code (adapted from Hundhausen, 1973).

faster than the fast mode (sound) speed, the interaction region can expand once shock formation occurs. Observations reveal that few CIRs are bounded by shocks at 1 AU (*e.g.*, Gosling *et al.*, 1972; Ogilvie, 1972), but that most are at heliocentric distances beyond ∼3 AU (*e.g.*, Hundhausen and Gosling, 1976; Gosling *et al.*, 1976; Smith and Wolfe, 1976). By 5 AU a large fraction of the mass and magnetic field flux in the solar wind flow at low heliographic latitudes is found within the interaction regions. At larger heliocentric distances stream speed amplitudes are greatly reduced, and the dominant structures are expanding compression regions that interact and merge with one another (*e.g.*, Burlaga, 1983; 1984).

5. Specific Comparison of Observations and Model Calculations

One can use solar wind measurements made near Earth as inputs to numerical codes to predict observed stream and CIR profiles at greater heliocentric distances. Such predictions can be compared directly with observations at larger distances when a distant spacecraft is nearly radially aligned with the Sun and Earth. Figure 5 illustrates the result of such a comparison using IMP 7 data at 1 AU, Pioneer 10 data at 4.7 AU, and the 1-D numerical code just described (Gosling *et al.*, 1976). The upper panel of the figure shows the solar wind speed profile measured near Earth by IMP 7 (the gap in the data is caused by passage of the spacecraft in the Earth's magnetosphere). The middle panel shows the speed profile of this same stream measured approximately 16 days later at 4.7 AU by Pioneer 10, then located slightly off the Sun-Earth line. In order to compare the two profiles, the Pioneer 10 data have been shifted in time in such a manner that the leading edge of the stream would be coincident at both spacecraft had the plasma on the leading edge of the stream propagated at constant speed from the Earth out to Pioneer 10. In fact, the stream arrived two days "early" at Pioneer 10, a consequence of the propagation of the CIR forward wave into the slower plasma ahead. In addition, the Pioneer 10 speed profile has a smaller amplitude (higher minimum speeds and lower maximum speeds) than the one at 1 AU, contains a forward-reverse shock pair on the rising speed portion of the profile that was not present at 1 AU, and shows a more gradual decline on its trailing edge. Finally, the high frequency structure present at 1 AU between days 6 and 10 is considerably damped in the Pioneer data.

The bottom panel of Fig. 5 shows the speed profile predicted at Pioneer 10 using the IMP 7 measurements of speed, density, and pressure as inputs to the 1-D gas dynamic code. The predicted and observed speed profiles are in reasonable agreement, although the calculation overestimates the amplitude of the shock transitions and underestimates the width of the CIR between the two shocks. [MHD and 2 and 3-D codes improve details of the agreement between model predictions and observations (*e.g.*, Dryer *et al.*, 1978; Pizzo, 1980).] It is of interest that the model predicts that the high frequency fluctuations present on the leading edge of the stream at 1 AU should be damped out by 4.7 AU, as observed. Small scale speed

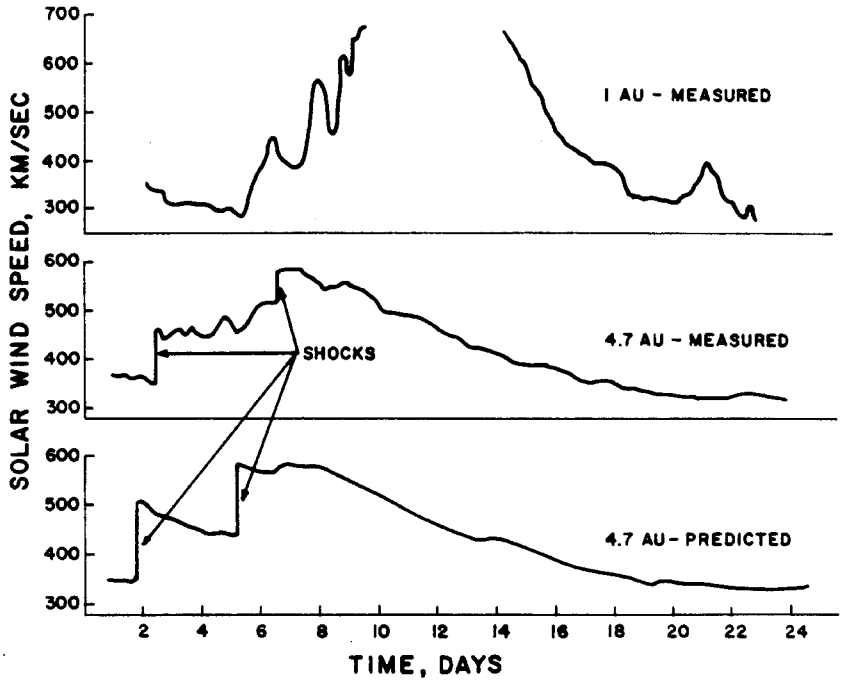

Figure 5. A comparison of the speed profiles of a solar wind stream observed first at 1 AU by IMP 7 and later at 4.65 AU by Pioneer 10, together with the stream profile at 4.65 AU predicted by a 1-D gas dynamic model. The 1 AU observations, using a linear interpolation across the data gap when IMP was in the magnetosphere, were used as the boundary conditions for the model calculation (from Gosling, 1986).

fluctuations are quickly wiped out as each sub-stream exchanges momentum with its immediate surroundings and is swept up by the longer wavelength stream. Thus the processes associated with CIR development and evolution act like a low-pass filter in the sense that only the longest wavelength speed structures survive at large heliocentric distances.

6. CIRs in Two Dimensions

Thus far we have seen that the basic physical processes associated with CIR development and evolution with increasing heliocentric distance can be understood from simple, 1-D gas dynamic considerations. However, CIRs are a consequence of spatial variation in the coronal expansion and solar rotation, and CIR formation and evolution is inherently 3-D in character. Moreover, magnetic forces help to determine the structure of CIRs. We begin our consideration of ever more complex details of CIRs by noting that when the coronal expansion is quasi-stationary but spatially variable, CIR evolution proceeds in an identical fashion at all solar

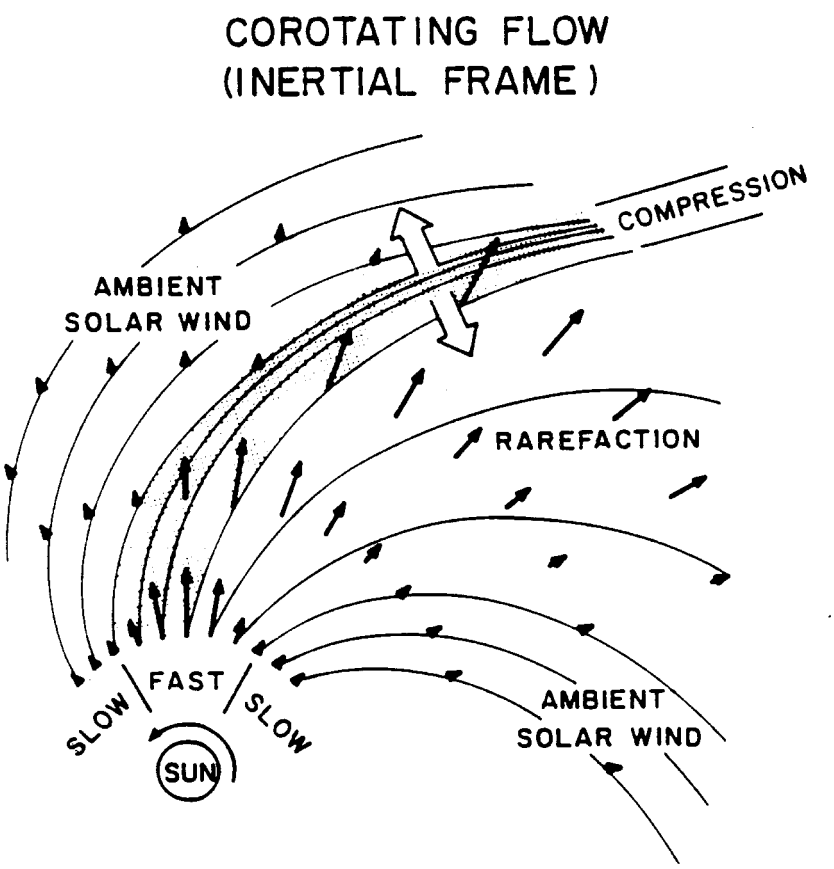

Figure 6. Schematic illustrating 2-D corotating stream structure in the solar equatorial plane in the inner heliosphere (from Pizzo, 1978).

longitudes in the equatorial plane; however, the state of evolution is a function of solar longitude. The pattern of interaction that develops in the equatorial plane is as shown by the sketch in Fig. 6 (Pizzo, 1978). It is worth emphasizing that although the pattern shown rotates with the Sun, each parcel of solar wind plasma moves outward nearly radially as indicated by the small arrows in the figure. Because CIRs are inclined relative to the radial direction, the pressure gradients associated with CIRs have both radial and azimuthal components as indicated by the large arrows in Fig. 6. Thus, the forward and reverse waves bounding a CIR have both radial and azimuthal components of propagation in the equatorial plane. In particular, the forward waves propagate antisunward and in the direction of planetary motion about the Sun (westward), while the reverse waves propagate sunward (in the plasma rest frame) and eastward. Consequently the slow wind is accelerated outward and deflected westward and the fast wind is decelerated and deflected eastward as a result of the interaction between the flows. This accounts for the

consistent pattern of west-east deflections observed within CIRs at 1 AU illustrated in Fig. 3. Indeed, those deflections have long been used to infer CIR and stream interface orientations in the equatorial plane (*e.g.*, Siscoe *et al.*, 1969; Gosling *et al.*, 1978). One consequence of the transverse deflections is that the plasma partially relieves the pressure build-up induced by stream steepening by simply slipping aside. Hence, CIRs evolve less rapidly than predicted by the simple 1-D calculation shown in Fig. 4 (*e.g.*, Pizzo, 1980), as can be seen in Fig. 5.

7. Latitudinal Variations

Until relatively recently direct measurements of the solar wind were limited to low heliographic latitudes, and our observational understanding of CIRs was essentially two-dimensional (2-D). The Ulysses polar journey about the Sun has, of course, changed our perceptions considerably. Ulysses' initial transit to high southern latitudes occurred at distances ranging between about 5.4 and 4.0 AU on the declining phase of the solar cycle. Beginning in July 1992, when Ulysses was at $\sim$S12°, the coronal magnetic field simplified considerably and approached that of a dipole tilted approximately 30° relative to the solar rotation axis (Hoeksema, 1995), much as illustrated in the upper left portion of Fig. 1. The alternating intervals of high and low-speed flow observed by Ulysses as it progressed southward to intermediate latitudes in 1992 and 1993, evident in Fig. 2, were a consequence of the simple tilted dipole present at that time (*e.g.*, Bame *et al.*, 1993). In 1996 and 1997 Ulysses returned to low latitudes at heliocentric distances again ranging from about 4.0 to 5.4 AU after having spent an extended interval at high northern latitudes. The solar magnetic field at this time was also simple, being roughly that of dipole oriented parallel to the rotation axis, much as illustrated in the lower left portion of Fig. 1. Alternating flows of high and low-speed wind were observed once again as Ulysses entered the band of solar wind variability at $\sim$N30° (Gosling *et al.*, 1997). In this case the alternating flows were associated more with a warping of the magnetic equator and the HCS than with dipole tilt.

CIRs were present on the leading edges of the high-speed streams in both hemispheres during these transits. As would have been expected from the Pioneer and Voyager observations, many of these CIRs were bounded by forward and/or reverse shocks. Figure 7 provides a summary of CIR shock observations during the transits to and from intermediate solar latitudes noted above. The figure shows a plot of the ratio of downstream to upstream density minus 1 as a function of solar latitude in both the southern (left) and northern (right) hemispheres. (The density ratio is a measure of shock strength and is inversely proportional to the ratio of upstream to downstream normal flow speeds in the shock frame.) Forward shocks are plotted above the horizontal line in each panel and reverse shocks are plotted below the line.

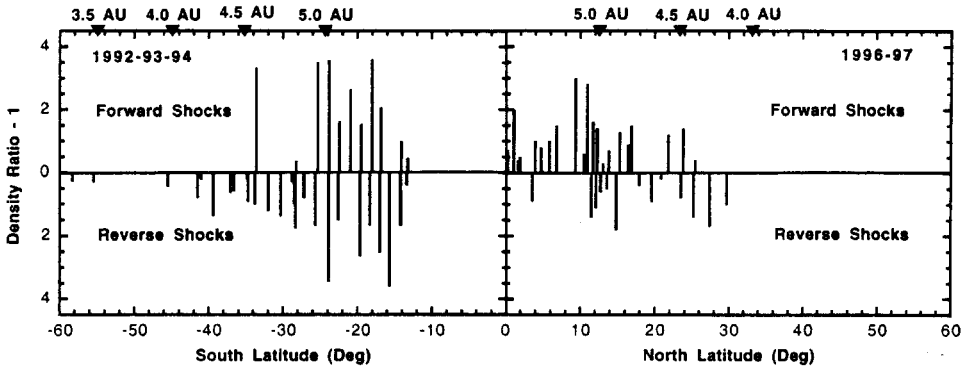

Figure 7. Shock "strength" versus latitude for corotating shocks observed during Ulysses' initial transit to high southern latitudes in 1992-93 (left) and during its return to low latitudes in 1996-97. Heliocentric distance is indicated at the top of the panels.

We note that the shocks in Fig. 7 often appear as forward-reverse shock pairs. However, during the southern transit Ulysses encountered only two CIR forward shocks poleward of S26° while it continued to encounter reverse shocks regularly up to a latitude of S42°, and sporadically thereafter to latitudes well above the band of solar wind variability where the interaction between fast and slow wind occurs (Gosling *et al.*, 1993; 1995a). It appears to be significant that the latitude (S26°) where the transition from shock pairs to only reverse shocks occurred is comparable to but slightly less than the inferred tilt of the solar magnetic dipole at that time. In general, the shocks observed above the band of variability were considerably weaker than their lower latitude counterparts, the weakest shocks being those observed at the highest latitudes. A somewhat similar, but less dramatic, pattern was observed at intermediate latitudes in the northern hemisphere in 1996 and 1997 when the solar magnetic dipole was far less steeply inclined to the solar rotation axis (Gosling *et al.*, 1997). Shock pairs were again seen at mid-latitudes, but above N26° only reverse shocks were observed. However, in this case the reverse shocks were not observed far above the band of variability. The shocks at all northern latitudes were generally weaker than their southern hemisphere counterparts in 1992 and 1993, and a preponderance of forward shocks was observed at latitudes below ∼N12° where the stream structure was highly irregular. We believe that differences between the shock patterns observed by Ulysses in the opposite solar hemispheres in 1992-93 and 1996-97 are associated primarily with the different solar magnetic dipole tilts at those times. Finally, we note that, consistent with the above observations, reverse waves that had not yet steepened into shocks were observed immediately poleward of both edges of the band of variability during Ulysses' rapid latitude scan at a heliocentric distance of ∼1.4 AU in early 1995 (Gosling *et al.*, 1995c).

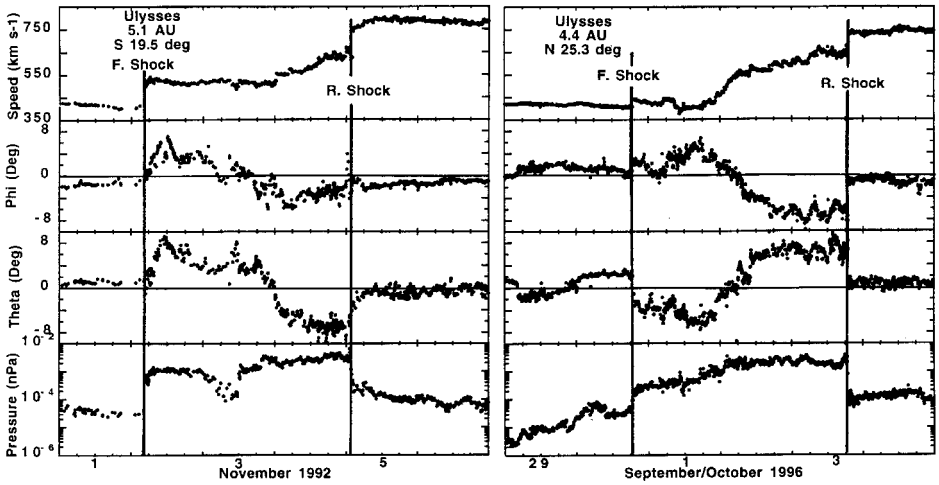

Figure 8. Typical corotating interaction regions observed in the southern (left) and northern (right) hemispheres by Ulysses. Parameters plotted are solar wind speed, azimuthal and meridional flow angles (positive for flow in the direction of planetary motion about the Sun and northward, respectively), and proton thermal pressure (adapted from Gosling *et al.*, 1995a; 1997).

8. Three-Dimensional Flow Deflections

Flow deflections observed downstream from the corotating shocks are central to understanding the physical origins of the above effects (Gosling *et al.*, 1993; 1997). Figure 8 shows selected solar wind plasma parameters for six-day intervals encompassing representative mid-latitude CIRs observed in the opposite solar hemispheres at large heliospheric distances by Ulysses. The forward shocks at the leading edges of these CIRs are distinguished in the data by abrupt increases in speed and pressure, while the reverse shocks at the trailing edges are distinguished by abrupt increases in speed and decreases in pressure (compare with the speed and pressure patterns evident in Fig. 4). The forward shocks were propagating into the slow wind ahead, while the reverse shocks were propagating back into the trailing high-speed plasma. Since both forward and reverse shocks are convected away from the Sun by the highly supersonic flow of the wind, Ulysses sampled the regions downstream of the forward shocks after shock passage and the regions downstream of the reverse shocks prior to shock passage.

As illustrated in Fig. 8, Ulysses commonly observed positive (westward) azimuthal (ϕ) flow deflections downstream of the forward shocks and negative (eastward) azimuthal flow deflections downstream from the reverse shocks in both hemispheres, as expected for CIRs. (Note the sign convention for the azimuthal flow in Figs. 3 and 8 is different.) Reversals in the azimuthal flow occurred near the centers of the CIRs. Of more interest here, the meridional (θ) deflections downstream from the shocks were of the opposite sense in the northern and southern

hemispheres. In the northern hemisphere the deflection pattern was southward at the forward shock and northward at the reverse shock, while in the southern hemisphere it was northward at the forward shock and southward at the reverse shock. Since a shock propagating through a fluid always deflects the fluid in the direction in which the shock is itself propagating, these flow changes indicate that not only were the forward shocks propagating antisunward and westward as expected, but they also were propagating equatorward in both hemispheres. Similarly, the reverse shocks were propagating sunward (in the plasma rest frame), eastward, and poleward in both hemispheres.

9. Tilted Interaction Regions

It is thus clear what causes the latitude occurrence of forward and reverse shocks apparent in Fig. 7. CIRs tend to have substantial and characteristic north-south tilts that are opposed in the two solar hemispheres. Typical shock tilts observed by Ulysses were of the order of 30° in both hemispheres (Riley *et al.*, 1996; Burton *et al.*, 1996; Gosling *et al.*, 1997). The tilts are such that the forward waves associated with CIRs propagate equatorward in both hemispheres; thus CIR forward shocks are seldom observed outside the band of solar wind variability. On the other hand, the reverse waves associated with CIRs propagate poleward in both hemispheres and can reach latitudes well above the band of variability, particularly when the solar magnetic dipole is inclined substantially to the solar rotation axis. The shocks are strongest at latitudes where the interaction is most directly driven by the interaction between fast and slow wind, and they weaken as they propagate to higher and lower latitudes.

10. Physical Origin of Opposed North-South Tilts

The opposed north-south tilts of CIRs arise because (1) the solar wind expansion near the Sun is controlled by the solar magnetic field, (2) the solar magnetic equator commonly is either tilted relative to the heliographic equator or contains substantial warps, or both, and (3) solar rotation drives CIRs (see, for example, Gosling, 1996). The sketch shown in Fig. 9 helps illustrate qualitatively how these factors combine to produce opposed north-south CIR tilts in the opposite solar hemispheres. Slow wind emanates from the region around and above the solar magnetic equator, which is tilted with respect to the heliographic equator either because of the magnetic dipole tilt or because the magnetic equator is warped. As the Sun rotates, the fast wind overtakes the slow wind in interplanetary space at interfaces (the stream interfaces) that are inclined relative to the solar equator in the same sense as is the magnetic equator (which maps outward to form the heliospheric current sheet). This compressive type of interaction occurs only where

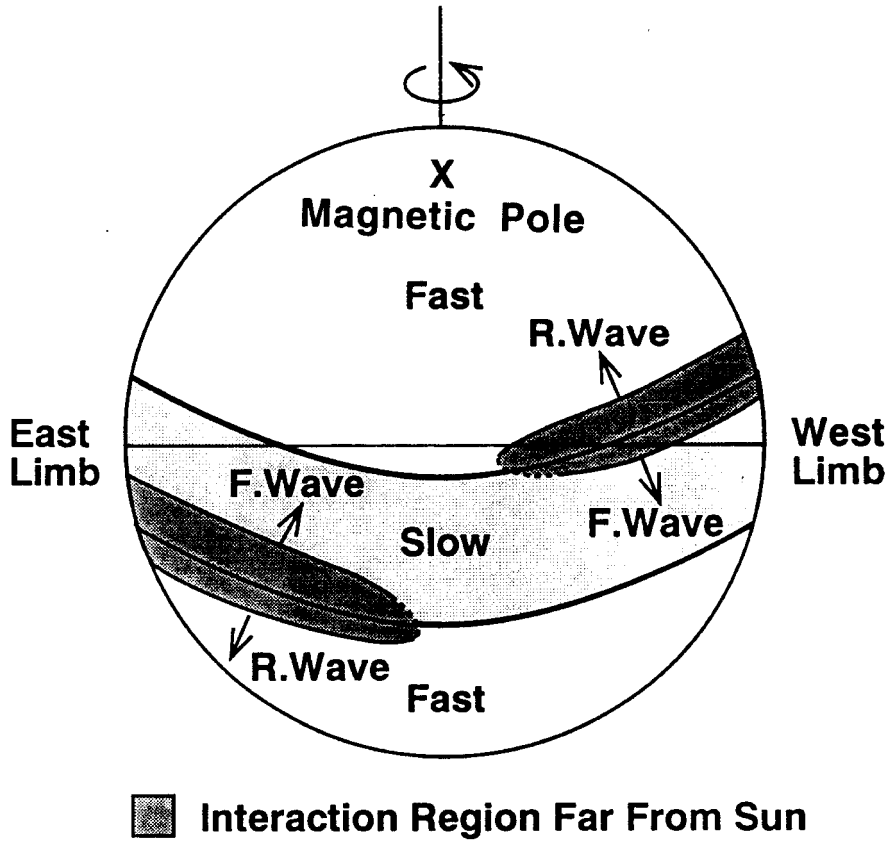

Figure 9. Sketch illustrating the origin of tilted CIRs. The pattern of flow is as established close to the Sun when the solar magnetic dipole is inclined substantially to the solar rotation axis. The interaction regions (heavy shade) develop well away from the Sun (from Gosling, 1996).

the interfaces are inclined poleward in going from left to right in the figure. Where the interfaces are inclined equatorward the interaction between fast and slow flow produces rarefactions. It is readily apparent that the stream interfaces and the CIRs in which they are embedded should have opposed north-south tilts in the northern and southern hemispheres. The forward and reverse waves bounding the CIRs always propagate roughly perpendicular to the interfaces; thus the forward waves in both hemispheres propagate antisunward, westward, and equatorward while the reverse waves propagate sunward (in the plasma rest frame), eastward, and poleward. Note that the stream interfaces are offset from, but are aligned roughly parallel to, the heliospheric current sheet; thus the HCS is not initially embedded within the CIRs. However, as the forward waves propagate into the slow wind they eventually overtake the HCS, which then becomes embedded within the CIRs. At 1 AU the HCS is found within a CIR in about two out of three cases (*e.g.*, Borrini *et al.*, 1981) and always precedes the stream interface (Gosling *et al.*, 1978). At distances beyond about 3 AU the HCS is virtually always embedded within a CIR.

11. Modeling CIRs in Three Dimensions

11.1. Observational Basis

As we have seen, the basic theoretical picture of CIR dynamics was well worked out with 1-D and 2-D models prior to Ulysses journey to high solar latitudes. It was also understood from simple geometric principles that the stream interaction process must weaken with latitude, as the rotational driving mechanism varies as $\sin\theta$, where θ is the colatitude (Siscoe, 1976). Hence, whatever the solar wind structure over the poles of the Sun, CIR activity should be inherently subdued at high heliocentric latitudes.

Nevertheless, there were many indications that the interplanetary expansion of the flow issuing from the warped, tilted-dipole magnetic structure of the corona must have consequences for the evolution of CIRs that are not included in planar models and that more was involved than simply $\sin\theta$. First, there were reliable remote-sensing observations of gross systematic latitudinal variations in global outflow properties. These include radio scintillation measurements that showed the flow speed was uniformly fast at high solar latitudes during the declining and minimum phases of the solar cycle (Sime, 1983), and Lyman-α backscatter observations which suggested significant pole-equator differences in mass flux (Lallement *et al.*, 1985). Together, such observations added consistency to the view that the magnetic structure of the corona, as deduced from visible and X-ray observations, governs the global solar wind flow. Second, a sometimes strong north-south component to the deflection at stream interfaces was noted in early 1 AU spacecraft observations and was interpreted in terms of meridional tilts of stream fronts (Siscoe, 1972). Third, one of the Pioneer (and later Voyager) spacecraft had, by the late 1970s, drifted sufficiently far off the ecliptic plane ($\sim 15^\circ$) to confirm the existence of significant persistent latitudinal differences in flow states (*e.g.*, Gazis *et al.*, 1989). Finally, even as Ulysses embarked upon its epic journey, a systematic pattern of large-scale north-south flow deflections were observed by Voyager 2 in the ecliptic plane at 20 AU near solar minimum; these were suspected as having something to do with the 3-D evolution of CIRs (McNutt, 1988).

Given the localized nature of spacecraft observations, full 3-D CIR simulations are required to provide the insights necessary to interpret data such as those collected by Ulysses. The simplest approach is to take advantage of the fact that since the flow is nearly radial in the hypersonic regime, one may approximate a true 3-D system by stitching together a set of 1-D or 2-D planar solutions across a range of latitudes (Suess *et al.*, 1975). This artifice captures the effect of the latitudinal variation in boundary conditions and the subsequent dynamics insofar as the nonradial propagation of pressure-driven phenomena can be ignored. To a first approximation, the low thermal and magnetic momentum densities in the interplanetary wind make this feasible, and the technique has been exploited for various applications (*e.g.*, Kóta, 1992). However, where strong compressions with

a substantial north-south tilt are involved and when considering propagation over long (AU or more) baselines, the approximation breaks down. Not only does the quantitative error become prohibitive, but certain effects are completely missing, such as the meridional propagation of disturbances to latitudes where the near-Sun flow is smooth and uniform and no interaction at all is expected on a planar basis.

11.2. Theoretical Underpinnings

Full dynamic treatment of 3-D CIRs hinges upon several key factors:

1. *Quasi-steady flow on the large scale.* The assumption is that there is a single frame rotating with the Sun in which the fast-slow flow pattern is fixed everywhere, *i.e.*, that all the fluid structures corotate at fixed angular rate. To the extent to which the global outflow pattern does not change appreciably over a flow time to any given heliocentric distance, this approximation is valid. It is usually assumed that solar wind structures corotate at the mean equatorial sidereal rate of 14.4° per day.

2. *The applicability of the ideal (M)HD description.* On the large scale, it is assumed that the interplanetary dynamics can be adequately described by the ideal MHD equations. This assumption appears even better justified in the interplanetary regime than in the corona, and it has been validated in a number of radial-alignment studies (*e.g.*, Pizzo *et al.*, 1995), in addition to those described earlier in this paper. In vector form, the MHD equations expressing conservation of mass, momentum, energy, and magnetic flux in a frame corotating with the Sun are given by:

$$\nabla \cdot \rho \mathbf{v} = 0 \tag{1}$$

$$\rho[(\mathbf{v}\cdot\nabla)\mathbf{v} + 2\Omega \times \mathbf{v} + \Omega \times (\Omega \times \mathbf{r})] = -\nabla P - \rho \frac{GM_s}{r^2}\hat{\mathbf{r}} + \frac{(\nabla \times \mathbf{B}) \times \mathbf{B}}{4\pi} \tag{2}$$

$$\nabla \cdot \left[\mathbf{v}\Big(\frac{1}{2}\rho(\mathbf{v}\cdot\mathbf{v} - |\Omega \times \mathbf{r}|^2) + \frac{\gamma}{\gamma - 1}P\Big) + \frac{\mathbf{B}}{4\pi} \times (\mathbf{v} \times \mathbf{B})\right] = -\rho \frac{GM_s v_r}{r^2}\hat{\mathbf{r}} \tag{3}$$

$$\nabla \cdot \mathbf{B} = 0\,. \tag{4}$$

The relevant physical quantities are the velocity, **v**, the magnetic field, **B**, the mass density, ρ, and the isotropic gas pressure, P. The latter is given by

$$P = 2nkT\,, \tag{5}$$

where n is the proton number density, k is the Boltzmann constant, and T is a single-fluid temperature. Mass density is usually taken to be the product of the proton mass and number density, n; however, the effects of heavier ions can be accounted for by using a mean ion mass. Constants include the solar sidereal rotation rate, Ω, the heliocentric distance, r, and the solar gravitational constant GM_s (gravitational effects are almost negligible in the interplanetary regime). The electrical conductivity is considered to be infinite, so that the field is frozen to the

flow; this means that in the corotating frame **v** and **B** are rigorously aligned. Although these equations are written in the corotating frame for physical clarity, they are generally solved in the inertial frame for computational reasons. The requisite transformation between **v** in the rotating frame and the velocity, **u**, in the inertial frame is given by

$$\mathbf{v} = \mathbf{u} - \Omega r \sin\theta \hat{\phi}\,, \tag{6}$$

where $\hat{\phi}$ is the azimuthal unit vector (in the direction of rotation).

3. *Restriction of the computational domain to the interplanetary regime.* The models typically situate the inner boundary of the computational domain some distance from the Sun, 18–30$R_\odot$, out where the flow is both supersonic and superalfvenic. This is partly because the physics of the outflow nearer the Sun is poorly known and partly because of mathematical considerations. Namely, inside the outermost critical point the formal boundary conditions are more complicated to deal with and require a much more demanding computational approach. Since physical conditions near the Sun can be only approximated at best, little is lost in restricting the problem to the interplanetary regime. In addition, the momentum-dominated character of the flow in interplanetary space ensures that specification of the internal energy equation is much less critical to the dynamics than in the corona. The problem is thus fundamentally simpler than in other solar/astrophysical systems, coming down to the application of a manageable set of conservation relations driven by a given set of boundary (or, more accurately, initial) conditions within an appropriate geometry. For this reason, the internal energy equation may comfortably be expressed via a polytropic relation between pressure and density; although this has the negative consequence that the thermodynamics is the most poorly modeled aspect of these models, it has minimal impact upon the overall dynamics.

The approximations invoked to make the computation more tractable come at some cost. All non-steady effects are completely lacking in the formulation. These obviously include impulsive disturbances and waves and instabilities of all kinds, but they also encompass slower secular change in the coronal sources, which may add up to something significant over sufficiently long propagation intervals. The magnetic field is treated in the mean laminar limit, so that the computed field topology takes no account of random walk effects (Jokipii and Davis, 1969). The neglect of differential rotation effects dictates a Parker spiral structure for the magnetic field, so that the topological connectivity concepts recently espoused by Fisk (1996) cannot self-consistently be addressed. Finally, the effects of pickup ions, which account for a significant fraction of the total pressure in the outer heliosphere (Gloeckler *et al.*, 1994) and thus may be important for CIR thermodynamics (Burlaga *et al.*, 1996), have yet to be included in 3-D CIR formulations. In all, some potentially significant processes and mechanisms are known to be lacking or poorly treated in 3-D – as in other – CIR simulations, so results are best viewed as valid on the large scale and at not too detailed a level. Moreover, cumulative computational error causes loss of accuracy in tracking individual structures over

vast distances, thus the focus of all such models must remain upon typical behavior and how well it describes the kinds of structures and phenomena actually observed.

11.3. Input Conditions

As will be seen shortly, the interplanetary CIR simulation is fully defined by specifying an appropriate set of flow variables on an inner boundary near the Sun. Spherical coordinates are the most practical choice for the problem, and it suffices to specify as a function of latitude and longitude the three components of velocity, the number density, the gas pressure, and the radial magnetic field strength on a spherical surface of heliocentric radius r_0.

Since there are no local measurements of these quantities for r_0 smaller than 0.3 AU, we must rely upon educated guesses as to the distribution of physical parameters to impose at r_0. A typical hypothetical representation of a tilted-dipole outflow is depicted in Fig. 10. A uniform band of slow, dense, cold outflow encircles the Sun at low heliographic latitudes, while uniform regions of fast, tenuous, hot outflow emanates from higher latitudes (*cf.* Fig. 9). Fast and slow regimes are separated by a relatively sharp transition. The slow flow band (taken to be the interplanetary extension of the streamer belt) is tilted at an angle α to the solar spin axis. This input structure has an improbable degree of simplicity and regularity, as compared with what we imagine the real flow distribution to be, but the dynamic and geometric content of the idealized pattern more than suffices to illustrate the essentials of 3-D CIR evolution. Indeed, given the abject simplicity of the inputs manifest in Fig. 10, the ensuing interplanetary complexity that evolves from it is truly remarkable, as we shall see shortly.

11.4. Numerical Integration

The numerical techniques employed to solve the above system of equations for the tilted-dipole input of Fig. 10 are detailed elsewhere (Pizzo, 1982), and we highlight here just one key aspect of the computational process. Namely, that by restricting the solution domain to the interplanetary regime, the MHD equations are everywhere hyperbolic. This means that the problem may be solved by recasting the vector equations in component form and using them to step the solution outwards in increments of Δr. The complete steady, 3-D flow pattern is thus built up as latitude-longitude distributions of the flow variables on successive spherical shells, integrating outwards as far as needed.

Since the solution is a 3-D volume of flow data, the analysis and interpretation of 3-D CIR simulations presents a visualization challenge. Nevertheless, through careful selection of cuts and slices through the overall solution, a good grasp of the dynamical structures contained can be acquired.

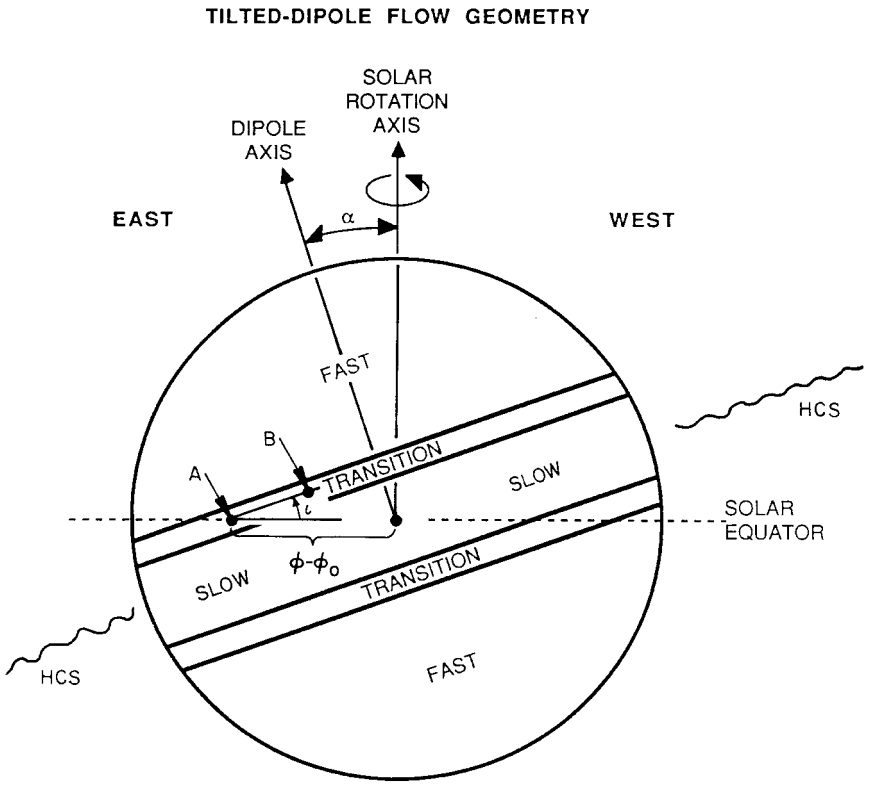

Figure 10. Schematic of the tilted-dipole flow geometry. The dipole axis is tilted from the solar rotation axis by an angle α, and the solar wind speed varies systematically along the direction parallel to the dipolar axis: fast flow comes from the poles of the dipole, slow solar wind from near the equator. The transition between fast and slow regimes is sharp, but not discontinuous, and flow conditions are presumed to be uniform in planes parallel to the dipolar equator. The angle ι defining the inclination of the stream front with respect to the equator is slightly less than α, by virtue of the longitudinal offset $\phi - \phi_o$ of the front from the line of nodes. The wavy lines marked "HCS" denote the heliospheric current sheet, which plays only an indirect role in the large scale interplanetary dynamics but which serves as a useful marker of what was originally slow wind near the Sun (from Pizzo, 1991).

11.5. 3-D Interface Structure and its Significance

The geometry of the interaction along the 3-D stream interface, the region where the two flow regimes collide, is the key to understanding the 3-D CIR evolutionary process as sketched in Fig. 9. The essential structure is illustrated in Fig. 11, where the interface is idealized as a smooth, thin surface. This surface separates fast flow (taken to lie on the sunward side of the surface) from the slow flow (near side) it is overtaking. It can be shown that relations between the tilt angle, the angles defining the interface orientation, and the jump in flow parameters across the interface can be derived from conservation relations (Pizzo, 1991). We focus here, however, on

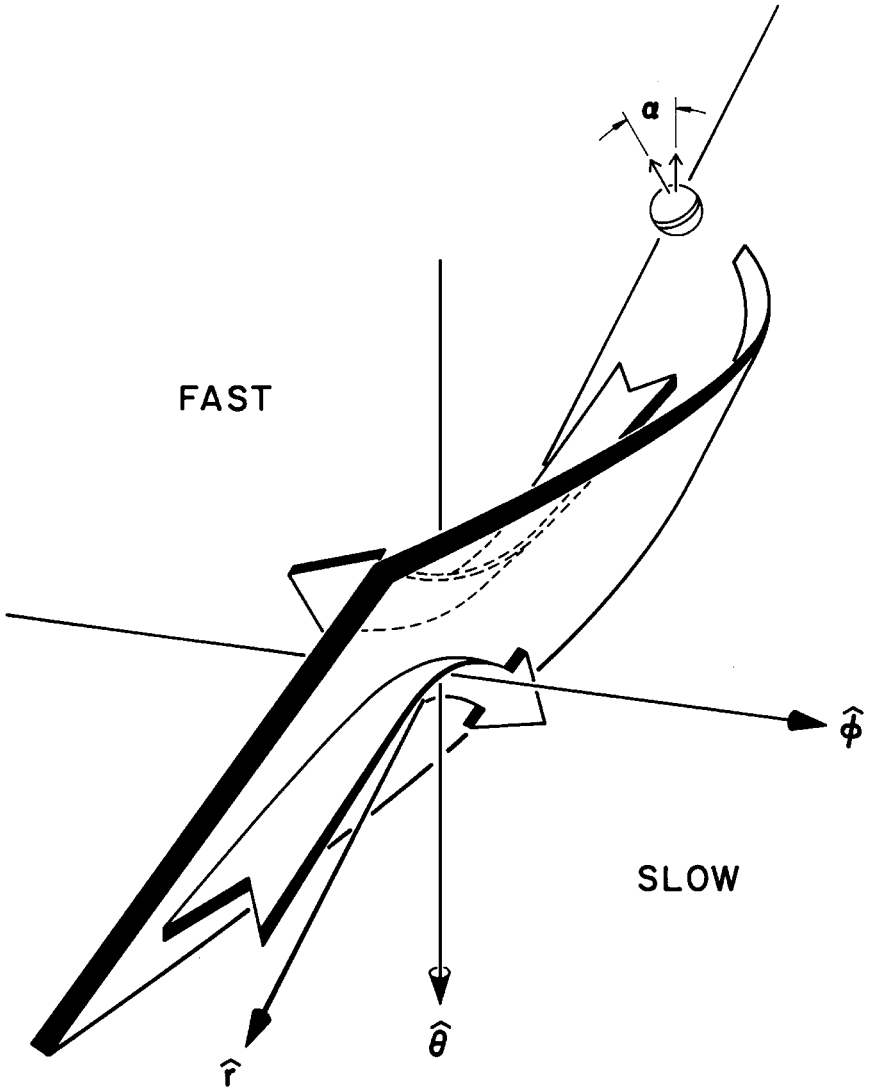

Figure 11. Interface orientation and relative flow geometry. To an observer riding along with the interface, slow fluid lying to the west (right) is swept into the interface from the near side, while fast fluid lying to the east (left) overtakes the interface from the far side. The slow fluid is deflected westward and southward (near white arrow, down) in the interaction, and the fast fluid is bent eastward and northward (far white arrow, up) (from Pizzo, 1991).

the fact that the interface is the site of strong shear flow, wherein the fast overtaking material is pushed eastward and northward (for the tilt of this interface), while the slow material is accelerated westward and southward. The turning of the plasma is effected by pressure gradients built up in the compressive overtaking of the flows, and it is well confirmed observationally that the total pressure does peak at the interface, where the flow directions shift abruptly about (*e.g.*, Fig. 3). The relative amplitude of the east-west and north-south deflections is a function of the dipole tilt angle and the interplanetary spiral angle at the interface location. The latter carries the implication that the north-south tilt of the stream front varies systematically with heliocentric distance, such that the front becomes increasingly perpendicular to the radial direction at large r.

As discussed in conjunction with 2-D CIR evolution, the shearing motions at the interface serve to cushion the interaction between the colliding flows. Where the dipole axis is inclined at a very small angle to the solar spin axis, as in the declining and minimum phases of solar activity, the cushioning effect is very efficient. In such cases, the pressure ridge built up between the streams grows slowly, and the large scale wave fronts which form the edges of the pressure ridge lie very oblique to the flow. Hence, corotating shock formation is retarded substantially.

The initial orientation of the stream interaction region varies systematically over the global structure of the tilted-dipole configuration. As viewed in Fig. 10, at the location where the interface crosses the equator, the north-south orientation of the interface surface relative to the heliographic equator (indicated by the line between points A and B) is essentially the dipole tilt angle. However, at higher latitudes the transition zone marking the locus of the interface surface turns over and lies flat along lines of constant heliographic latitude (see also Fig. 9). At these locations, there is initially no stream interaction at all, since it is a pure shear flow. Thus in any 3-D configuration, some parts will be evolving more slowly and others more rapidly, depending not only upon the magnitude of the velocity difference, but also upon the initial 3-D orientation of the interface separating fast and slow flows. In a simple configuration like Fig. 10, it is meaningful to talk as if the evolution is defined entirely by the dipole tilt angle, but, in general, when the slow flow band topology is more convoluted the evolution is more complicated.

11.6. 30° Tilt Simulation

Fortified with this knowledge, we present in Fig. 12 an example of a tilted-dipole simulation conducted with input conditions that roughly approximate those obtaining during the Ulysses south polar pass. The dipole tilt angle at that time was about 30°, and high and low speed flows were about 750 and 300 km/s, respectively. The figure shows latitude-longitude maps of outflow velocity V at 1 and 5 AU. High speed shows as bright, low speed as dark. The thin line tracing through the slow flow band near the equator marks the locus of the HCS. (In these maps, the sense of the corotational advection is for fast flow to advance to the right.) In the

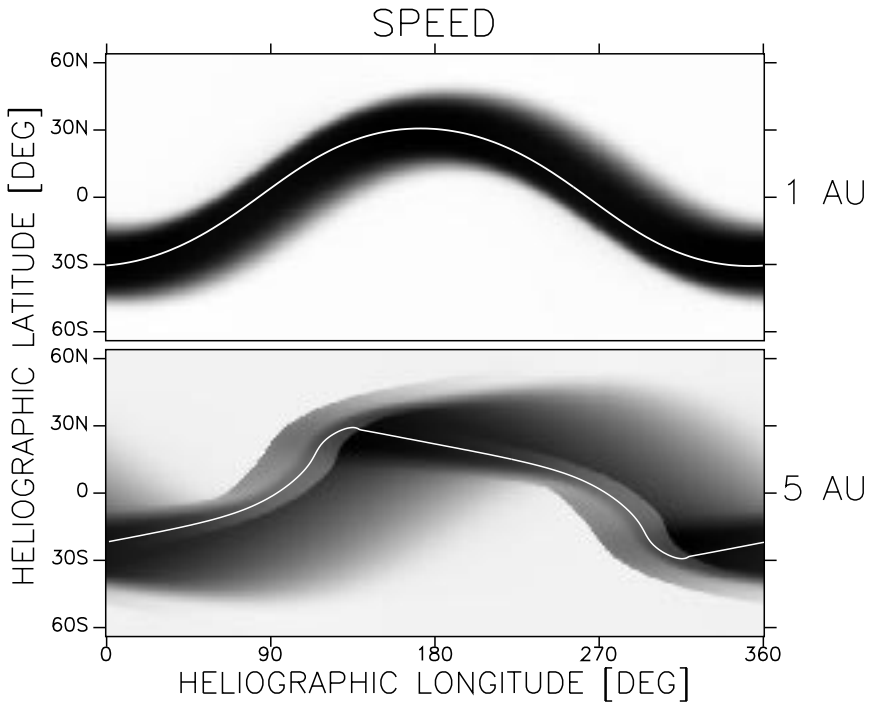

Figure 12. Latitude-longitude gray-scale map of velocity at 1 AU and 5 AU. Light/dark shading indicates high/low speed flow. The white sinusoid line near the equator represents the HCS. In the lower panel, the flow pattern has been shifted 90° in longitude to compensate for the corotational drift between 1 and 5 AU. CIRs at 5 AU appear as the two medium-tone diagonal features near 90° and 270° longitude. The abrupt velocity changes bordering the CIRs are forward/reverse shock pairs. Note that the reverse shock (forming the left border, in each case) extends to higher latitudes than does the forward shock (right borders) (from Pizzo and Gosling, 1994).

top panel, the flow system has evolved little (because of the uniform idealization and the shallow tilt of the slow flow band) in transit from the tilted-dipole initial surface (Fig. 10) at $r_0 = 0.15$ AU. By 5 AU (lower panel), however, significant structure has evolved. A forward-reverse shock pair has formed at the leading edge of the northerly stream in the region around the HCS (near 90° longitude), and, by virtue of the input symmetry, a mirror image CIR has formed at the front of the southerly stream (near 270°). The trailing edge of the southerly stream shows as the graduated shadowy structure extending from 90–180° longitude near the equator; an identical feature associated with the northerly stream is centered near the 0–360° fold in the map. Thus, although the form of the velocity structures is the same in both hemispheres, the geometry causes their north-south inclinations to be opposed, as in Fig. 9.

Inspection of Fig. 12 reveals a striking consistency with the observed statistical distribution of shock occurrences depicted in Fig. 7: both forward and reverse shocks are seen at low latitudes, but forward shocks weaken and ultimately disap-

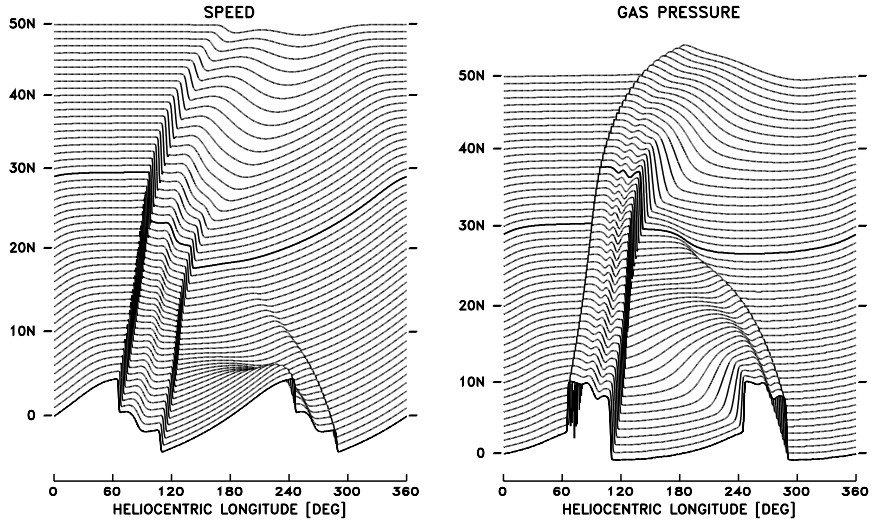

Figure 13. Series of traces taken at 1° intervals in latitude through the 5 AU velocity (left) and gas pressure (right) structure. The view is looking north from the equator, and a spacecraft would sample the flow from right to left. The dark trace lies at λ_{HCS} (the actual value at 5 AU, both in the observations and in the simulation, is $\lambda_{HCS} = 29°$), highlighting the abrupt disappearance of the shock front above that latitude (from Pizzo and Gosling, 1994).

pear at latitudes above the maximum poleward excursion of the HCS. The reverse shock, however, extends well above this latitude.

The penetration of the reverse shock to latitudes outside the limits of the input slow flow band, up where there was initially no azimuthal structure at all, is a specifically 3-D dynamic property – it cannot be replicated in any meaningful way by latitudinal stacking of planar flows. The weakening and disappearance of the forward shock with increasing latitude is due in part to the input boundary conditions alone, but there is also a subtle component to this mechanism that is purely 3-D in origin. This effect is seen in Fig. 13, which provides a slightly different perspective on the data plotted in Fig. 12. The figure consists of a series of traces, taken at 1° latitude intervals, of the velocity and gas pressure viewed in a projection where the height of the trace indicates the magnitude of the flow parameter. At the equator the streams are identical, as imposed by symmetry, but one stream (north, in this case) dominates at higher latitudes. Forward and reverse shocks stand out as steep bunchings of the trace lines, with the less discontinuous velocity jump at the interface clearly visible in between. (The gas pressure undergoes a jump at the interface, since it separates gases of different origin, but the total pressure profile peaks across the interface.) The extension of the northerly reverse shock to high latitudes is evident, as is the weakening and disappearance of the forward shock near the latitude of the HCS. Contributing to the decay of the forward shock is the pressure wave running up from the forward wave of the southerly stream, which interacts with and weakens the northern forward shock. This sort of ex-

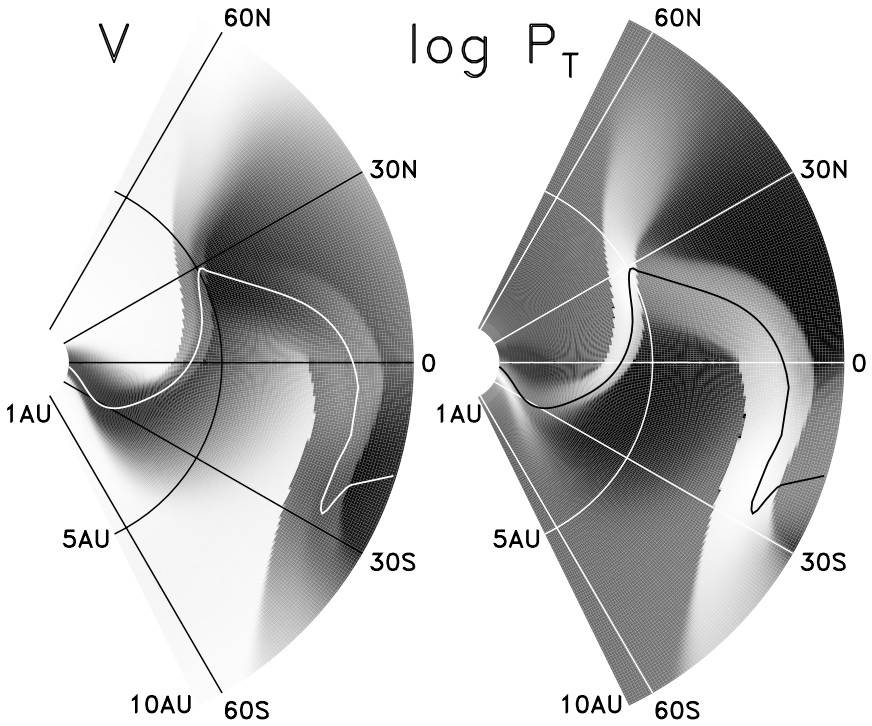

Figure 14. North-south slice through the tilted-dipole flow pattern between 1 and 10 AU. Velocity is shown at left, log of the total pressure at right. High values are indicated by light shading, low values by dark; the HCS is the line weaving back and forth across the equator. Note the distortion of the HCS that results from fast flow pushing into slow flow, the latitudinal extent of the CIR fronts, and the interaction of the northern stream with the trailing edge of the preceding southern stream (from Pizzo and Gosling, 1994).

tended, cross-latitudinal interaction leads to great complexity in CIR structure at large heliocentric distances (Pizzo, 1994a, 1994b).

The cross-latitudinal interaction is directly seen in Fig. 14, which is a north-south cut through the 3-D flow structure of Fig. 12 at approximately 90° longitude. The high-pressure fringe of the southern CIR projects into the path of the forward shock of the northern stream near the top of the HCS. Also visible in Fig. 14 is the distension and warping of the HCS by the interaction between the high and low-speed flows (Pizzo, 1994b), the north-south tilts of the CIR structures, and their extension well beyond the peak latitude of either the HCS or the initial poleward limits of the slow-flow band.

Rarefaction regions associated with the trailing edge of high-speed streams are an intimate part of the interplanetary dynamics of CIRs. As the CIRs strengthen due to the interaction of slow and fast flows in the innermost heliosphere, they begin to expand and push into the surrounding medium. At low latitudes in Fig. 12, the forward shock associated with the northern CIR has run much of the way through what was originally the slow flow material in front of it and is about to propagate

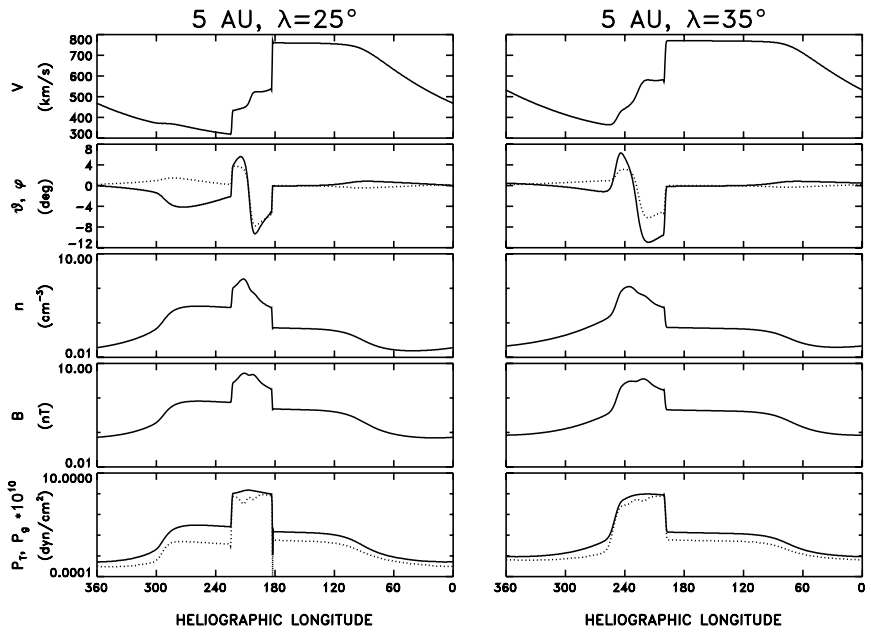

Figure 15. Simulated spacecraft trace at 5 AU, just equatorward (left) and poleward (right) of λ_{HCS}. From top are shown speed, north-south (ϑ, solid) and east-west (ϕ, dotted) flow angles; on a log scale, the next three panels display number density, magnetic field intensity, and total pressure (solid) and gas pressure (dotted) (from Pizzo and Gosling, 1994).

up the trailing edge of the preceding southerly stream in its path. The negative velocity gradients there weaken the forward shock. There is less rarefactive effect near the broad, high-latitude top of the slow flow band, but this region, too, is gradually being eroded from the front (west) by the trailing edge of the preceding arm of the northerly high speed stream. In addition, the rarefactions associated with the streams at low latitudes are themselves expanding laterally, so additional latitudinal erosion takes place.

Folding together what is depicted in Figs. 12 and 14, one gains an impression of the relation of the overall dynamic structure of CIRs to the warped heliospheric current sheet. Although the center of interaction between the fast and slow flows is the stream interface rather than the HCS, which merely serves as a tracer of the original flow geometry close to the Sun, the HCS is eventually swept into and distorted by the CIRs. Moreover, the basic (distorted) ballerina skirt structure of the HCS is reflected in the global geometry of the CIRs.

How well such simulations correspond to real solar wind flows may be judged by comparison of Figs. 8 and 15. Figure 15 shows simulated 5 AU spacecraft cuts, at two different latitudes, through the flow patterns of the above figures. Qualitatively, all the observed morphological features of 3-D CIRs are replicated in the computation, and the quantitative correspondence is quite good considering there was no attempt to fine tune the input parameters.

11.7. GENERALIZATION

The above example serves well to illustrate the basic dynamics associated with idealized tilted-dipole configurations. However, even within the strictures of the idealization, both quantitative and, to some extent, qualitative results are affected by the choice of inputs, such as the fast/slow velocity difference, the dipole tilt angle, and the angular thickness and mass and momentum flux contrast of the slow flow band relative to the fast flow. Partial consideration of these variations has been addressed (Pizzo, 1994a), from which several conclusions can be drawn. First, as the tilt angle increases, the interaction fronts become inclined at greater angles to the heliocentric equator. The interaction becomes more nearly 2-D in character, with the entire process evolving much more rapidly as a function of heliocentric distance. In addition, for an idealized planar streamer belt configuration oriented perpendicular to the heliographic equator, the latitudinal band subjected to direct CIR activity spreads toward the poles to include most of the 4π sphere. Thus strong CIR shocks envelop the entire inner heliosphere, with true 3-D effects prominent only at the highest latitudes. Conversely, when the dipole tilt angle is very small, the stream-stream interaction is very oblique and weak, with shock formation taking place several AU farther out and significant CIR activity being confined to a relatively narrow band about the heliocentric equator. Elements of the tilt-angle effect can be glimpsed in Fig. 7: the tilt was substantially smaller during Ulysses' north polar pass, and this is reflected by the weaker shocks and smaller latitudinal spread in the plot. In fact, when the tilt is very small around solar minimum, discrete warps in the streamer belt structure drive the most readily observable CIR disturbances, such as detected by Ulysses in late 1996 and on into 1997. That is, large-amplitude, long-wavelength, steady undulations in the tilted-dipole structure spawn localized streams of greater effective tilt than that associated with the mean planar structure of the slow flow band. Thus, a 20° bump in a planar, 5° tilted-dipole will produce a CIR characteristic of a 20° tilted-dipole flow.

12. 3-D CIRs in the Distant Heliosphere

The above discussion pertains to CIRs in the inner heliosphere, which evolve as discrete entities. Depending upon input tilts, velocity differences, etc., at $\sim$10 AU the forward and reverse waves of successive spiral arms of the global CIR pattern begin to collide (*e.g.*, Gosling, 1986; Whang and Burlaga, 1988). The interaction is driven by the expansion of the high-pressure ridges built up by the overtaking of fast and slow flows closer to the Sun, with the maximum of the compression typically occurring inside $\sim$5–7 AU. Because of the opposed tilts of the CIRs in the opposite hemispheres, the CIR-CIR interaction commences at mid-latitudes for a planar tilted-dipole configuration (see, for example, Fig. 14), then spreads toward the equator. The sequence of events is depicted in Fig. 16, which is from a simulation similar to that depicted in Fig. 12 ($\alpha = 30^\circ$), but with slightly lower overall

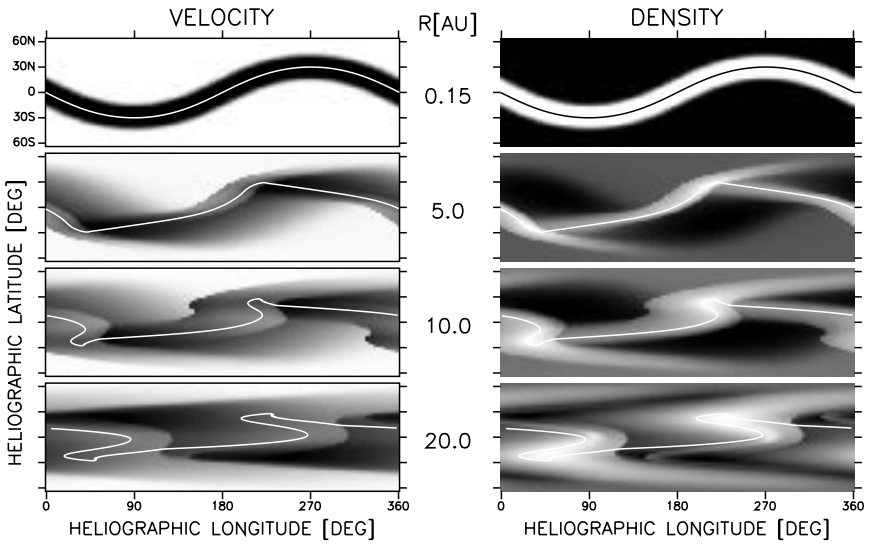

Figure 16. 3-D MHD simulation of an $\alpha = 30°$ tilted-dipole flow to 20 AU, in the format of Fig. 12. The expanding, medium-gray features in the lower three panels denote 3-D CIR structures, bounded sharply right and left by inclined, forward/reverse shock surfaces. Note the interactions between forward and reverse CIR fronts that take place beyond 10 AU and the dynamic complexity that has evolved from so simple an input (from Pizzo, 1994b).

velocities. By 10 AU the CIRs have expanded out to cover $\sim 90°$ of heliocentric longitude, and interactions between the forward and reverse waves are occurring at the fringes of each structure. By 20 AU, forward and reverse wave fronts have swept completely through each other at low latitudes, with only the forward waves surviving. This is consistent with Voyager 2 observations in the ecliptic during the declining and minimum phases of the solar cycle (Burlaga, 1994). The CIRs visible near the equator in the density plot are actually secondary CIR structures, consisting of material that has been shocked in the CIR-CIR interaction. At high latitudes, no such interaction takes place, since the reverse shock of each original CIR has propagated outside the zone of interactions. The reverse shocks are prevented by the geometric divergence of the geometry from progressing much farther toward the poles (see, for example, Riley *et al.*, 1996), and they gradually weaken with heliocentric distance. Note also that the initial close correspondence between the velocity structures and the location of the HCS has been lost in the CIR-CIR interactions.

The interactions and the complexity of the flow pattern continue to evolve with heliocentric distance, since the momentum exchange at the remaining shock fronts is slight and they decay only slowly (Hundhausen, 1973). The limitations of the numerical model preclude accurate estimation of where the shocks eventually die out. Their decay may be determined by processes not included in the basic MHD description, such as mass loading by pickup ions (Burlaga *et al.*, 1997).

13. Conclusion

The basic mechanisms of CIR evolution fleshed out over the last two decades were given a considerable boost by the observations of Ulysses. However, many lingering questions remain. Even within the context of the idealized modeling approaches covered in this paper, many facets of the problem have yet to be explored. For example, it would be of considerable utility to map out in detail the run of shock strengths, locations, and orientations for key examples, and the behavior in the distant heliosphere has been probed only in an exploratory manner. The consequences of pickup ions and the treatment of the internal energy equation need to be investigated, as well as the implications of the magnetic field line connectivity concepts recently developed by Fisk (1996). Finally, the effects of allowing slow changes in the global flow pattern (non-stationarity) to account for the secular evolution of the coronal outflow are yet unknown. Indeed, establishing the range of applicability of the entire picture of CIRs summarized in this paper during the rise of solar activity will be a prime objective of the Ulysses extended mission.

Acknowledgements

Work at Los Alamos was performed under the auspices of the U.S. Department of Energy with support from NASA. Work at NOAA was performed under the auspices of the U.S. Department of Commerce with support from NASA.

References

Bame, S. J., Goldstein, B. E., Gosling, J. T., Harvey, J. W., McComas, D. J., Neugebauer, M., and Phillips, J. L.: 1993, 'Ulysses Observations of a Recurrent High Speed Stream and the Heliomagnetic Streamer Belt', *Geophys. Res. Lett.* **20**, 2323–2326.

Belcher, J. W., and Davis, L.:1971, 'Large-Amplitude Alfvén Waves in the Interplanetary Medium - II.', *J. Geophys. Res.* **76**, 3,534–3,563.

Borrini, G., Gosling, J. T., Bame, S. J., Feldman, W. C., and Wilcox, J. M.: 1981, 'Solar Wind Helium and Hydrogen Structure near the Heliospheric Current Sheet - A Signal of Coronal Streamers at 1 AU', *J. Geophys. Res.* **86**, 4,565–4,573.

Bruno, R., Villante, U., Bavassano, B., Schwenn, R., and Mariani F.: 1986, 'In-situ Observations of the Latitudinal Gradients of the Solar Wind Parameters during 1976 and 1977', *Sol. Phys.* **104**, 431–445.

Burlaga, L. F.: 1974, 'Interplanetary Stream Interfaces', *J. Geophys. Res.* **79**, 3,717–3,725.

Burlaga, L. F.: 1983, 'Corotating Pressure Waves without Fast Streams in the Solar Wind', *J. Geophys. Res.* **88**, 6,085–6,094.

Burlaga, L. F.: 1984, 'MHD Processes in the Outer Heliosphere', *Space Sci. Rev.* **39**, 255–316.

Burlaga, L. F.: 1994, 'Shocks in the Outer Heliosphere: Voyager 2 Observations from 18.9 AU to 30.2 AU (1986–1989)', *J. Geophys. Res.* **99**, 4,161–4,171.

Burlaga, L. F., Ness, N. F., Belcher, J. W., and Whang, Y. C.: 1996, 'Pickup Protons and Pressure-Balanced Structures from 39 to 43 AU: Voyager 2 Observations during 1993 and 1994', *J. Geophys. Res.* **99**, 15,523–15,532.

Burlaga, L. F., Ness, N. F., and Belcher, J. W.: 1997, 'Radial Evolution of Corotating Merged Interaction Regions and Flows between ∼14 AU and ∼43 AU', *J. Geophys. Res.* **102**, 4,661–4,671.

Burton, M. E., Smith, E. J., Balogh, A., Forsyth, R. J., Bame, S. J., Phillips, J. L., and Goldstein, B. E.: 1996, 'Ulysses out-of-Ecliptic Observations of Interplanetary Shocks', *Astron. Astrophys.* **316**, 313–322.

Carovillano, R. L., and Siscoe, G. L.: 1969, 'Corotating Structure in the Solar Wind', *Sol. Phys.* **8**, 401–414.

Coles, W. A.: 1995, 'Interplanetary Scintillation Observations of the High-Latitude Solar Wind', *Space Sci. Rev.* **72**, 211–222.

Dryer, M., Smith, Z. K., Smith, E. J., Mihalov, J. D., Wolfe, J. H., Steinolfson, R. S., and Wu, S. T.: 1978, 'MHD Modeling of Solar Wind Corotating Stream Interaction Regions Observed by Pioneer 10 and 11', *J. Geophys. Res.* **83**, 4,347–4,352.

Feldman, W. C., Asbridge, J. R., Bame, S. J., Fenimore, E. E., and Gosling, J. T.: 1981, 'The Solar Origin of Solar Wind Interstream Flows: Near Equatorial Coronal Streamers', *J. Geophys. Res.* **86**, 5,408–5,416.

Fisk, L. A.: 1996, 'Motion of the Footpoints of Heliospheric Magnetic Field Lines at the Sun: Implications for Recurrent Energetic Particle Events at High Heliographic Latitudes', *J. Geophys. Res.* **101**, 15,547-15,553.

Gazis, P. R., Mihalov, J. D., Barnes, A., Lazarus, A. J., and Smith, E. J.: 1989, 'Pioneer and Voyager Observations of the Solar Wind at Large Heliocentric Distances and Latitudes', *Geophys. Res. Lett.* **16**, 223–226.

Gloeckler, G., Geiss, J., Roelof, E. C., Fisk, L. A., Ipavich, F. M., Ogilvie, K. W., Lanzerotti, L. J., von Steiger, R., and Wilken, B.: 1994, 'Acceleration of Interstellar Pickup Ions in the Disturbed Solar Wind Observed on Ulysses', *J. Geophys. Res.* **99**, 17,637–17,643.

Gosling, J. T.: 1986, 'Global Aspects of Stream Evolution in the Solar Wind', *in* R. I. Epstein and W. C. Feldman (eds.), *Magnetospheric Phenomena in Astrophysics*, AIP Conf. Proceed. **144**, New York, pp. 124–144.

Gosling, J. T.: 1996, 'Corotating and Transient Solar Wind Flows in Three Dimensions', *Ann. Rev. Astron. Astrophys.* **34**, 35–73.

Gosling, J. T., Hundhausen, A. J., Pizzo, V., and Asbridge, J. R.: 1972, 'Compressions and Rarefactions in the Solar Wind: Vela 3', *J. Geophys. Res.* **77**, 5,442–5,454.

Gosling, J. T., Hundhausen, A. J., and Bame, S. J.: 1976, 'Solar wind Stream Evolution at Large Heliocentric Distances: Experimental Demonstration and Test of a Model', *J. Geophys. Res.* **81**, 2,111–2,122.

Gosling, J. T., Asbridge, J. R., Bame, S. J., and Feldman, W. C.: 1978, 'Solar Wind Stream Interfaces', *J. Geophys. Res.* **83**, 1,401–1,412.

Gosling, J. T., Borrini, G., Asbridge, J. R., Bame, S. J., Feldman, W. C., and Hansen, R. F.: 1981, 'Coronal Streamers in the Solar Wind at 1 AU', *J. Geophys. Res.* **86**, 5,438–5,448.

Gosling, J. T., Bame, S. J., McComas, D. J., Phillips, J. L., Pizzo, V. J., Goldstein, B. E., and Neugebauer, M.: 1993, 'Latitudinal Variation of Solar Wind Corotating Stream Interaction Regions: Ulysses', *Geophys. Res. Lett.* **20**, 2789–2792.

Gosling, J. T., Bame, S. J., McComas, D. J., Phillips, J. L., Pizzo, V. J., Goldstein, B. E., and Neugebauer, M.: 1995a, 'Solar Wind Corotating Interaction Regions out of the Ecliptic Plane: Ulysses', *Space Sci. Rev.* **72**, 99–104.

Gosling, J. T., Bame, S. J., Feldman, W. C., McComas, D. J., Phillips, J. L., Goldstein, B. E., Neugebauer, M., Burkepile, J., Hundhausen, A. J., and Acton, L.: 1995b, 'The Band of Solar Wind Variability at Low Heliographic Latitudes near Solar Activity Minimum: Plasma Results from the Ulysses Rapid Latitude Scan', *Geophys. Res. Lett.* **22**, 3329–3332.

Gosling, J. T., Feldman, W. C., McComas, D. J., Phillips, J. L., Pizzo, V. J., and Forsyth, R. J.: 1995c, 'Ulysses Observations of Opposed Tilts of Solar Wind Corotating Interaction Regions in the Northern and Southern Solar Hemispheres', *J. Geophys. Res.* **22**, 3,333–3,336.

Gosling, J. T., Bame, S. J., Feldman, W. C., McComas, D. J., Riley, P., Goldstein, B. E., and Neugebauer, M.: 1997, 'The Northern Edge of the Band of Solar Wind Variability, Ulysses at ∼4.5 AU', *Geophys. Res. Lett.* **24**, 309–312.

Hoeksema, J. T.: 1995, 'The Large-Scale Structure of the Heliospheric Current Sheet during the Ulysses Epoch', *Space Sci. Rev.* **72**, 137–148.

Hundhausen, A. J.: 1972, *Coronal Expansion and Solar Wind*, Springer-Verlag, New York.

Hundhausen, A. J.: 1973, 'Nonlinear Model of High-Speed Solar Wind Streams', *J. Geophys. Res.* **78**, 1,528–1,542.

Hundhausen, A. J.: 1977, 'An Interplanetary View of Coronal Holes', *in* J. B. Zirker (ed.), *Coronal Holes and High Speed Wind Streams*, Colorado Assoc. Univ. Press., Boulder, pp. 225–329.

Hundhausen, A. J., and Gosling, J. T.: 1976, 'Solar Wind Structure at Large Heliocentric Distances: An Interpretation of Pioneer 10 Observations', *J. Geophys. Res.* **81**, 1,436–1,440.

Jokipii, J. R., and Davis, L. Jr.: 1969, 'Long-Wavelength Turbulence and the Heating of the Solar Wind', *Astrophys. J.* **156**, 1101–1106.

Jokipii, R. J., and Thomas, B.: 1981, 'Effects of Drift on the Transport of Cosmic-Rays - IV. Modulation by a Wavy Current Sheet', *Astrophys. J.* **243**, 1115–1122.

Kóta, J.: 1992, 'A Numerical Model of the Large-Scale Solar Wind in the Outer Heliosphere', *in* E. Marsch and R. Schwenn (eds.), *Solar Wind Seven*, Pergamon, New York, pp. 205–208.

Krieger, A. S., Timothy, A. F., and Roelof, E. C.: 1973, 'A Coronal Hole and its Identification as the Source of a High Velocity Solar Wind Stream', *Sol. Phys.* **29**, 505–525.

Lallement, R., Bertaux, J. L., and Kurt, V. G.: 1985, 'Solar Wind Decrease at High Heliocentric Latitudes Detected from Prognoz Interplanetary Lyman-α Mapping', *J. Geophys. Res.* **90**, 1,413–1,423.

McNutt, R. L., Jr.: 1988, 'Possible Explanations of North-South Plasma Flow in the Outer Heliosphere and Meridional Transport of Magnetic Flux', *Geophys. Res. Lett.* **15**, 1523–1526.

Ogilvie, K. W.: 1972, 'Corotating Shock Structures', *in* P. J. Coleman, C. P. Sonett, and J. M. Wilcox (eds.), *Solar Wind*, NASA SP **308**, Washington DC, pp. 430–434.

Parker, E. N.: 1963, *Interplanetary Dynamical Processes*, John Wiley, New York.

Phillips, J. L., Balogh, A., Bame, S. J., Goldstein, B. E., Gosling, J. T., Hoeksema, J. T., McComas, D. J., Neugebauer, M., Sheeley, N. R., and Wang, Y.-M.: 1994, 'Ulysses at 50° South: Constant Immersion in the High-Speed Solar Wind', *J. Geophys. Res.* **21**, 1,105–1,108.

Pizzo, V. J.: 1978, 'A Three-Dimensional Model of Corotating Streams in the Solar Wind - I. Theoretical Foundations', *J. Geophys. Res.* **83**, 5,563–5,572.

Pizzo, V. J.: 1980, 'A Three-Dimensional Model of Corotating Streams in the Solar Wind - II. Hydrodynamic Streams', *J. Geophys. Res.* **85**, 727–743.

Pizzo, V. J.: 1982, 'A Three-Dimensional Model of Corotating Streams in the Solar Wind - III. Magnetohydrodynamic Streams', *J. Geophys. Res.* **87**, 4,374–4,394.

Pizzo, V. J.: 1991, 'The Evolution of Corotating Stream Fronts near the Ecliptic Plane in the Inner Solar System - II. Three-Dimensional Tilted-Dipole Fronts', *J. Geophys. Res.* **96**, 5,405–5,420.

Pizzo, V. J.: 1994a, 'Global, Quasi-Steady Dynamics of the Distant Solar Wind - I. Origins of North-South Flows in the Outer Heliosphere', *J. Geophys. Res.* **99**, 4,173–4,183.

Pizzo, V. J.: 1994b, 'Global, Quasi-Steady Dynamics of the Distant Solar Wind - II. Deformation of the Heliospheric Current Sheet', *J. Geophys. Res.* **99**, 4,185–4,191.

Pizzo, V. J., and Gosling, J. T.: 1994, 'Three-dimensional Simulation of High-Latitude Interaction Regions: Comparison with Ulysses Results', *Geophys. Res. Lett.* **21**, 2063–2066.

Pizzo, V. J., Intriligator, D. S., and Siscoe, G. L.: 1995, 'Two-dimensional Radial-Alignment Simulation of Solar Wind Streams Observed by Pioneer 10 and 11 in 1974', *J. Geophys. Res.* **100**, 12,251–12,260.

Pneuman, G. W., and Kopp, R. A.: 1971, 'Gas-Magnetic Field Interactions in the Solar Corona', *Sol. Phys.* **18**, 258–270.

Richter, A. K., and Luttrell, A. H.: 1986, 'Superposed Epoch Analysis of Corotating Interaction Regions at 0.3 and 1.0 AU: A Comparative Study', *J. Geophys. Res.* **91**, 5,873–5,878.

Riley, P., Gosling, J. T., Weiss, L. A., and Pizzo, V. J.: 1996, 'The Tilts of Corotating Interaction Regions at Mid-Heliograhic Latitudes', *J. Geophys. Res.* **101**, 24,349-24,357.

Sarabhai, V.: 1963, 'Some Consequences of Nonuniformity of Solar-Wind Velocity', *J. Geophys. Res.* **68**, 1,555–1,557.

Schwenn, R.: 1990, 'Large-Scale Structure of the Interplanetary Medium', *in* R. Schwenn and E. Marsch (eds.), *Physics of the Inner Heliosphere*, Springer-Verlag, Berlin Heidelberg, pp. 99–181.

Sime, D. G.: 1983, 'Interplanetary Scintillation Observations of the Solar Wind Close to the Sun and out of the Ecliptic', *in* M. Neugebauer (ed.), *Solar Wind Five*, NASA CP **2280**, pp. 453–467.

Siscoe, G. L.: 1972, 'Structure and Orientation of Solar Wind Interaction Fronts: Pioneer 6', *J. Geophys. Res.* **77**, 27–34.

Siscoe, G. L.: 1976, 'Three-Dimensional Aspects of Interplanetary Shock Waves', *J. Geophys. Res.* **81**, 6,235–6,241.

Siscoe, G. L., Goldstein, B., and Lazarus, A. J.: 1969, 'An East-West Asymmetry in the Solar-Wind Velocity', *J. Geophys. Res.* **74**, 1,759–1,762.

Smith, E. J., and Wolfe, J. H.: 1976, 'Observations of Interaction Regions and Corotating Shocks between One and Five AU: Pioneers 10 and 11', *J. Geophys. Res.* **3**, 137-140.

Suess, S. T., Hundhausen, A. J., and Pizzo, V.: 1975, 'Latitude-Dependent Nonlinear High-Speed Solar Wind Streams', *J. Geophys. Res.* **80**, 2,023–2,029.

Whang, Y. C., and Burlaga, L. F.: 1988, 'Evolution of Recurrent Solar Wind Structures between 14 AU and the Termination Shock', *J. Geophys. Res.* **93**, 5,446–5,460.

Wimmer-Schweingruber, R. F., von Steiger, R., and Paerli, R.: 1997, 'Solar Wind Stream Interfaces in Corotating Interaction Regions: SWICS/Ulysses Results', *J. Geophys. Res.* **102**, 17,404-17,417.

Zhao, X. P., and Hundhausen, A. J.: 1981, 'Organization of Solar Wind Plasma Properties in a Tilted, Heliomagnetic Coordinate System', *J. Geophys. Res.* **86**, 5,423–5,430.

Address for Offprints: J. T. Gosling, Los Alamos National Laboratory, MS D466, Los Alamos, NM 87545, USA.